The Chihuahua dog, a new animal model for Neuronal Ceroid Lipofuscinosis CLN7 disease?

Kiterie M. E. Faller[1], Jose Bras[2], Samuel J. Sharpe[1], Glenn W. Anderson[3], Lee Darwent[2], Celia Kun-Rodrigues[2], Joseph Alroy[4], Jacques Penderis[5], Sara E. Mole[6], Rodrigo Gutierrez-Quintana[1*], Rita J. Guerreiro[2*]

*** Joint senior authorship**

1. School of Veterinary Medicine, College of Medical, Veterinary and Life Sciences, University of Glasgow, Bearsden Road, Glasgow, G61 1QH, UK
2. Department of Molecular Neuroscience, Institute of Neurology, University College London, Queen Square, London, WC1N 3BG, UK
3. Department of Histopathology, Great Ormond Street Hospital, London, WC1N 3JH, UK
4. Department of Pathology, Tufts University School of Medicine and Tufts-New England Medical Center, Boston, Massachusetts 02111, USA
5. VetExtra Neurology, Craig Leith Road, Broadleys, Stirling, FK7 7LE, UK
6. MRC laboratory for Molecular Cell Biology, UCL institute of Child Health, and Department of Genetics, Evolution and Environment, University College London, Gower Street, London, WC1E 6BT, UK

Running head: The Chihuahua dog, a model for CLN7 disease

Associate editor: Dr Aurora Pujol Onofre

Keywords: MFSD8, lysosomal storage disorder, neurodegeneration

Corresponding author: Tel.: +44 141 3305848; fax: +44 141 3303663; *Email address:* Rodrigo.GutierrezQuintana@glasgow.ac.uk (Rodrigo Gutierrez-Quintana)

Support information: This study was funded by a grant from the University of Glasgow Small Animal Hospital Fund. J.B. and R.J.G. are supported by fellowships from the Alzheimer's Society.

An abstract of part of this work has been submitted for presentation at the Annual Congress of the European College of Veterinary Neurology.

ABSTRACT

Neuronal ceroid lipofuscinoses (NCL) are a group of incurable lysosomal storage disorders characterized by neurodegeneration and accumulation of lipopigments mainly within the neurons. We studied two littermate Chihuahua dogs presenting with progressive signs of blindness, ataxia, pacing and cognitive impairment from the age of one year old. Due to worsening of clinical signs, both dogs were euthanized at around two years of age. Post-mortem examination revealed marked accumulation of autofluorescent intracellular inclusions within the brain, characteristic of NCL. Whole genome sequencing was performed on one of the affected dogs. Following sequence alignment and variant calling against the canine reference genome, variants were identified in the coding region or splicing regions of four previously known NCL genes (*CLN6*, *ARSG*, *CLN2=TPP1* and *CLN7=MFSD8*). Subsequent segregation analysis within the family (two affected dogs, both parents and three relatives) identified *MFSD8*:p.Phe282Leufs13* as the causal mutation, which had previously been identified in one Chinese crested dog with no available ancestries. Due to the similarities of the clinical signs and histopathological changes with the human form of the disease, we propose that the Chihuahua dog could be a good animal model of CLN7 disease.

SIGNIFICANCE STATEMENT

NCL are a group of incurable lysosomal storage disorders unified by similar histopathological changes. Although mutations in 13 genes coding for functionally distinct proteins have been identified, the pathophysiology of these diseases is still poorly understood. Naturally occurring large animal models have had an invaluable contribution to better understand the pathophysiology and therapeutic options of some forms of NCL. CLN7 is a poorly characterized form, and this could be due to a lack of animal models that closely reproduce the human phenotype. We identified Chihuahua dogs with a genetic mutation causing CLN7 disease, which could represent an excellent animal model.

INTRODUCTION

Neuronal Ceroid Lipofuscinoses (NCL) are a heterogeneous group of inherited lysosomal storage disorders characterized by neurodegeneration and accumulation of autofluorescent lipopigments mainly in neurons. In human patients, they represent the most prevalent hereditary neurovisceral storage disorder with an incidence of 1.3 to 7 for every 100,000 live births, depending on the country (Mole and Williams, 2001 [Updated 2013]). Symptoms usually include blindness, motor and cognitive decline, seizures and premature death. The disease was originally classified on the basis of age of onset and clinical signs into congenital, infantile, late-infantile, juvenile and adult forms, with many possible variants (Mole and Williams, 2001 [Updated 2013]; Shacka, 2012). More than 400 different mutations in thirteen genes have been identified in human patients, and three genes have recently been suggested as – unproven – candidate genes (Di Fruscio et al., 2015). Despite coding for functionally distinct proteins − some soluble and some transmembrane proteins − mutations of these genes all induce accumulation of autofluorescence storage material (Shacka, 2012). Mutations in different genes can result in similar phenotypes, whereas different mutations in the same gene can lead to a very different disease course. This rendered the original classification based on age of onset of limited value. The current characterization of NCL forms is now based on the causative mutation (Mole and Williams, 2001 [Updated 2013]).

Numerous animal models of NCLs have been described and have been invaluable in contributing to the current understanding of this devastating condition. However, despite extensive research, the disease mechanisms are still not fully understood and animal models provide the opportunity to further understand the pathophysiology and

assess new therapeutic strategies for each different form. In veterinary medicine, NCL has been described in various species including the sheep, cow, goat, horse, ferret, cat and dog (Jolly and Palmer, 1995; Anderson et al., 2013). In dogs, the causative mutation has been found in many breeds, including the American Bulldog (*CLN10*) (Awano et al., 2006), Border Collie (*CLN5*) (Melville et al., 2005), English Setter (*CLN8*) (Katz et al., 2005a), Dachshund (*CLN1* and *CLN2*) (Awano et al., 2006; Sanders et al., 2010), Tibetan Terrier (*ATP13A2* = *CLN12*) (Farias et al., 2011; Wohlke et al., 2011), Australian Shepherd (*CLN6*) (Katz et al., 2011), Golden Retriever (*CLN5*) (Gilliam et al., 2015), Australian Shepherd mix (*CLN8*) (Guo et al., 2014) and more recently strongly suspected in a single Chinese Crested dog (*MFSD8* = *CLN7*) (Guo et al., 2015). Mutation in *ARSG* (*Arylsulfatase G*) has also been identified in the American Staffordshire Bull Terrier suffering from a lysosomal storage disorder initially classified as NCL (Abitbol et al., 2010); however, more recent reports suggest that ARSG-deficiency should be referred as a mucopolysaccharidosis (more precisely MPS IIIE) (Kowalewski et al., 2012; Kowalewski et al., 2015). Multiple sporadic reports of Chihuahua dogs affected by NCL exist (Rac and Giesecke, 1975; Kuwamura et al., 2003; Nakamoto et al., 2011), but, to date, the causative mutation has not been identified.

We present here a family of Chihuahua dogs with a progressive neurological disease confirmed to be a form of NCL after histopathologic and ultrastructural examinations. After generating a whole genome sequence using DNA from one of the affected dogs, a mutation in *MFSD8* (*CLN7*) gene was identified and this was confirmed by segregation analysis in the related dogs. The Chihuahua dog could represent a new animal model for CLN7 disease.

MATERIAL AND METHODS

1. Patient cohort – Clinical investigations

Two littermate Chihuahua dogs (one male and one female) were presented to the Small Animal Hospital, University of Glasgow, for investigation of progressive neurological signs. Following clinical examination and routine complete blood count and biochemistry, they underwent magnetic resonance imaging (MRI) of the brain under general anesthesia. MR images were acquired using a 1.5 T (64 MHz) system (Magnetom Essenza, Siemens, Camberley, UK). T2-weighted, Fluid-attenuated inversion recovery, T2*-weighted, and T1-weighted images prior and after contrast were acquired in sagittal, transverse and dorsal planes. Routine cerebrospinal fluid analysis including total nucleated cell count, cytology and protein measurement was performed in the two affected cases and urinary organic acid screening by mass spectrometry was performed in the male dog.

2. Histopathology and electron microscopy

The male dog was euthanized at 1 year 11 months of age and underwent a full post-mortem examination. Representative samples from the cerebrum and cerebellum were fixed in 2.5 % glutaraldehyde for electron microscopy (EM) analysis and other samples from the cerebrum and cerebellum were embedded in Tissue-Tek O.C.T (Sakura) and snapped frozen in isopentane chilled in liquid nitrogen before being stored at -80 °C for fluorescence microscopy. The rest of the brain, the eyes, and samples from skin, liver, kidney, adrenal, spleen, heart, duodenum and pancreas were fixed in 10 % buffered formalin. Slices of the formalin-fixed brain were then embedded in paraffin, before staining with hematoxilin and eosin (H&E), PAS, Sudan blue and Luxol fast blue. Samples for fluorescence microscopy were analysed as

145 previously described (Katz et al., 2005b). Immunostaining was performed using
146 antibodies directed against glial fibrillary acid protein (GFAP) and lysosomal-
147 associated membrane protein 1 (LAMP-1) (see Table I for details of antibodies used).
148
149 3. Family analysis – Ethical statement
150 The breeder of the affected dogs was contacted and agreed to provide DNA samples
151 in the form of cheek swabs from the parents of the dogs and from related family
152 members (Fig. 1). EDTA blood samples were available from the two affected dogs.
153 Approval from the local ethical committee (University of Glasgow, School of
154 Veterinary Medicine) was granted (Form Ref. 12a/14) for this study.
155
156 4. Molecular analysis
157 DNA was extracted from the blood of the two affected animals using a DNeasy Blood
158 and Tissue kit (Qiagen, Crawley, UK) and from the cheek swabs using a Gentra
159 Puregene Buccal Cell Kit (Qiagen, Crawley, UK).
160 Whole-genome sequencing was performed on the affected female dog using
161 Illumina's TruSeq PCR free protocol according to the manufacturer's instructions
162 combined with Illumina's Hiseq2000 on paired-end 100bp reads. Sequence alignment
163 and variant calling were performed against the dog genome reference CanFam3.1
164 using bwa (Li and Durbin, 2009) and the Genome Analysis Toolkit respectively
165 (McKenna et al., 2010; DePristo et al., 2011), largely following the Best Practices v3,
166 with hard filters for variant recalibration. In short, this consisted of duplicate read
167 marking, realignment around indels, base quality score recalibration, variant
168 identification using the HaplotypeCaller tool. High quality variants were annotated
169 using snpEff (Cingolani et al., 2012) against the dog reference CanFam3.1.75.

The data were initially analyzed for known NCL genes. Given the apparent autosomal recessive mode of transmission of the disease in the family, homozygous variants in the coding exons or splicing regions of previously described NCL genes were prioritized. Variants were identified in *CLN6*, *ARSG*, *TPP1* and *MFSD8* genes. Segregation analysis for these candidates was performed by Sanger sequencing. Following PCR amplification (see Table II for mutation location and primers used), the PCR products were purified using ExoSAP-IT (USB), before direct Sanger sequencing of both strands using BigDye Terminator v.3.1 chemistry v.3.1 (Applied Biosystems) and an ABI 3730XL Genetic Analyzer (Applied Biosystems). Sequencing traces were analyzed with Sequencher software v.4.2 (Gene Codes).

RESULTS

1. Clinical description of the patients

The affected Chihuahua dogs were a 1-year 10 month old male neutered and a 2-year 1 month old female at the time of presentation. The male started to demonstrate clinical signs at 1 year 4 months of age and the female at one year of age. They both demonstrated progressive vision deficits, pacing and behavioral changes. On examination, the dogs appeared disorientated, poorly responsive and were bumping into objects. They were ataxic on all limbs and had a wide-based stance. The female dog also demonstrated an intermittent right head tilt. Proprioceptive positioning was normal and there were mildly delayed hopping responses in all limbs. Segmental spinal reflexes were normal. Menace responses were absent bilaterally with intact dazzle reflexes and normal pupillary light reflexes. Remaining cranial nerves examination, segmental spinal reflexes and vertebral column palpation were within normal limits. No significant abnormalities were detected on physical examination,

195 including eye fundus examination. A complete blood count and biochemistry were
196 mainly unremarkable, with the exception of a moderate increase in liver enzymes and
197 bile acid stimulation tests in the male dog (Alanine aminotransferase: 372 IU/L –
198 reference interval (RI) <90; aspartate aminotransferase: 55 IU/L – RI<40; pre-
199 prandial bile acids: 5.3 μmol/L – RI<5 and post prandial bile acids: 50 μmol/L –
200 RI<15). MRI in both cases demonstrated a severe dilatation of the entire ventricular
201 system of the brain. The interthalamic adhesion appeared markedly decreased in size;
202 the cerebellar sulci and the fissures between the cerebellar folia were noticeably
203 widened. These changes suggested marked brain atrophy (Fig. 2A). Cerebrospinal
204 fluid (CSF) analysis was unremarkable. Urine organic acids were measured by mass
205 spectrometry in the male dog and were not suggestive of a disorder of organic acid
206 metabolism.
207 In light of the MRI changes, breed and in the absence of CSF abnormalities, a storage
208 disease, and more specifically NCL, was highly suspected. The dogs were discharged
209 with no treatment and the owners were warned of the very poor prognosis. Due to the
210 deterioration of the clinical signs, both owners elected for euthanasia of their dogs
211 within a month of discharge, but only the owners of the male dog agreed to post-
212 mortem examination.
213
214 2. Histopathological features
215 On gross examination of the brain, a moderate and symmetrical dilation of the lateral
216 ventricles was noted, associated with a thin cortex. Histopathological examination
217 demonstrated widespread amorphous to globular, eosinophilic to golden-brown,
218 intracytoplasmic storage material within neurons and astrocytes within the cerebral
219 cortex, basal ganglia, hippocampus, thalamus, brainstem and cerebellum (Fig. 2 and

3). All storage material within astrocytes and neurons stained variably magenta with Periodic Acid-Schiff (PAS), variably positive with Sudan blue and intensively positive with Luxol fast blue (Fig. 2C and D). When viewed under a microscope equipped for epifluorescence illumination, as previously described (Katz et al., 2005b), inclusion material fluoresced brightly (Fig. 2E). In the cortical grey matter neuronal necrosis was absent but neuronal density was reduced and remnant laminar neurons were disarrayed, and associated with an increased number of reactive astrocytes and activated microglia. Within the cerebellum, Purkinje cells contained abundant intracytoplasmic storage material. There was some disorganization and a subjectively moderate decrease in the number of Purkinje cells, and several of the remaining Purkinje cells showed a mildly shrunken with hypereosinophilic cytoplasm and pyknotic nuclei (degeneration). Granular layer neurons were markedly reduced in density (Fig. 3). Neurons within the pyramidal layer of the hippocampus contained abundant intracytoplasmic storage but were present in normal numbers. Immunohistochemical staining confirmed the marked neuroinflammation with a high number of GFAP-positive astrocytes (Fig. 2G). Moreover, the tissue showed strong staining against LAMP-1 (lysosomal-associated membrane protein 1), indicative of alterations in this protein of the lysosome membrane (Fig. 2F). Finally, ganglion cells within the retina were markedly reduced in number and when present contained abundant intracytoplasmic storage material (Fig. 2I). Storage material was also found in the duodenum, liver and heart using PAS staining and immunohistochemistry against LAMP-1.

Based on these characteristics, NCL was diagnosed. NCL is a heterogeneous group of diseases, and further characterization involves ultrastructural analysis of the storage

material. EM showed a complex multilamellar profile with presence of curvilinear and rectilinear profiles (Fig. 2H).

3. Molecular analysis

Non synonymous mutations in the following previously known NCL genes were identified: *ARSG* (p.Val262Asp, *CLN6* (p.Lys29Arg), *TPP1* (rs22973585) and *MFSD8* (p.Phe282Leufs13*). *ARSG*, *CLN6* and *TPP1* variants did not segregate with the disease phenotype and were therefore excluded as the causative mutations. The *MFSD8* single pair deletion segregated within the available members of the family, with affected dogs being homozygous for the mutation, both clinically unaffected parents heterozygous for the mutation and clinically unaffected relatives either heterozygous for the mutation or homozygous for the wild-type allele (Fig. 4). This mutation is predicted to result in a severely truncated protein, which further supports this to be the causal mutation.

DISCUSSION

In this study, we describe a family of dogs diagnosed with a mutation in *MFSD8* (*CLN7*) resulting in neuronal ceroid lipofuscinosis. The mutation is predicted to induce a frame shift leading to a premature stop codon.

The two littermates were monitored for clinical signs of degenerative brain disease, mainly for the development of blindness, ataxia and cognitive impairment. These changes, secondary to marked brain atrophy, are very similar to those observed in patients affected with NCL or other animal forms of the disease. Presence of typical autofluorescent cytoplasmic inclusions associated with marked neuronal loss and astrocytosis confirmed the diagnosis of NCL. Numerous sporadic reports of

Chihuahua dogs affected with NCL have been described in the literature with a total number of six previously described cases (Rac and Giesecke, 1975; Kuwamura et al., 2003; Nakamoto et al., 2011). Similarities in age of onset, clinical signs and nature of the inclusion make it likely that these animals were affected by the same mutation as the dogs presented here. The previous descriptions concerned Chihuahua dogs from Japan and Australia, which suggests a world-wide distribution of the mutation. It may also be possible that the disease is not recognized by veterinarians, or that it is confused with other diseases such as hydrocephalus that is relatively common in the breed and can present with similar clinical signs. A commercial diagnostic test should be considered in order to determine the frequency of the mutations and to eradicate it from the breed.

Interestingly, the same mutation has recently been strongly suspected as the cause of NCL in a single dog of another breed, the Chinese Crested, although lack of family ancestry did not allow further confirmation by segregation analysis (Guo et al., 2015). Our report is a further confirmation of this previously identified mutation. The clinical signs, age of onset, imaging and pathologic findings were very similar to that described here. The prevalence of the mutation in the Chinese crested population was extremely low (only one heterozygous animal out of 1478 tested Chinese crested), which makes it unlikely that a carrier animal could be found to start a colony to use as animal model. The presence of the identical mutation in the two breeds would suggest a common ancestor for the affected Chinese crested and Chihuahua dogs, possibly through another dog breed from Mexico, the Mexican hairless dog (Xoloitzcuintle). The Mexican hairless dogs and Chinese crested dogs are hairless dog breeds, which are very likely to be related as they carry an identical mutation at the origin of their alopecia (Drogemuller et al., 2008).

294

295 To identify the mutation, we sequenced the whole genome of one of the affected dogs
296 and compared it with the canine reference genome sequence. This allowed us to scan
297 initially for sequence variants in the coding and splicing regions of the canine
298 orthologs of the previously known genes to cause NCL in human patients. This
299 approach has been previously reported by others and was successful at finding
300 mutations causing NCL in dogs (Guo et al., 2014; Gilliam et al., 2015; Guo et al.,
301 2015). One of the genes (*ARSG*) considered as a candidate gene for NCL has now
302 been re-classified as causative of a form of mucopolysaccharidosis (MPS IIIE)
303 (Kowalewski et al., 2012; Kowalewski et al., 2015). However, the close proximity of
304 these neurodegenerative disorders made exclusion of a mutation in this gene
305 important.

306

307 In human patients, mutations in the *CLN7/MFSD8* gene generally result in a late-
308 infantile form, now called CLN7 disease. Symptoms are usually first noted between
309 the age of 2 to 7 years with seizures and developmental regression. Progression of the
310 disease results in motor and mental impairment, and blindness, leading to premature
311 death occurring before adulthood in most patients (Kousi et al., 2012). Despite being a
312 significant cause of late-infantile NCL in people (Aiello et al., 2009), very little is
313 known about the pathophysiology of CLN7, which is in part due to (until recently) the
314 lack of suitable animal models (Damme et al., 2014). MFSD8 is a lysosomal
315 membrane protein belonging to the major facilitator superfamily (MFS). It is thought
316 to act as a transporter but its substrate is still currently unknown (Damme et al., 2014).
317 A mouse model of *Mfsd8* disruption has been created and should contribute to a better
318 understanding of this form of NCL, especially regarding the function of the protein

and the disease mechanisms. Unfortunately, this model has limitations, as it does not accurately reproduce the clinical and histopathological findings seen in human patients (Damme et al., 2014). No obvious neuronal loss is observed in these mice, although marked accumulation of autofluorescent material in the nerve cells and retinal degeneration (photoreceptor layer) is evident. The failure to reproduce all key-features of the human disease may be due to the presence of residual Cln7 protein function in these mice. In contrast, the Chihuahua dogs presented here could represent a better model as the histopathologic findings mimic the human pathology with marked neuronal loss and astrocytosis, resulting in progression of neurological signs incompatible with life (Table III). In the dog presented here, the Purkinje cells layer appears relatively spared - although signs of degeneration are visible – compared to what is observed in human patients. This difference could be due to the fact that the dog has been euthanized at a reasonably early stage of the disease. Indeed, this layer tends to be progressively lost in patients contrary to the granular cells layer, which is completely lost at very early age (Elleder et al., 2011). Overall, canine models are a good complement to murine models, especially for assessment of potential therapies due to a closer phenotype and longer lifespan (Faller et al., 2015). Additionally, the Chihuahua breed would be a particularly promising model due to its reasonably small size and ease of handling, which would make them particularly suitable as research individuals. However, further histological characterization of dogs of both sexes and of different ages would be needed for a better understanding of the progression of the disease.

In conclusion, we have identified a mutation in *MFSD8* causing Neuronal Ceroid Lipofuscinosis in Chihuahua dogs. This breed could represent a good animal model of CLN7 disease.

CONFLICT OF INTEREST STATEMENT

The authors have no conflict of interest to declare.

ROLES OF AUTHORS

All authors had full access to the data in the study and take responsibility for the integrity of the data and the accuracy of the data analysis.

KF examined one of the affected dogs, genotyped and sequenced samples from some variants and drafted the manuscript. JB conceived the mutation identification strategy, identified the variants in the sequence alignment and drafted the manuscript. SS performed the post-mortem and histopathological examinations and interpreted the pathologic findings. GWA performed advanced histological analysis. LD and CKR genotyped and sequenced samples from some variants. JA interpreted electron microscopy findings. JP supervised the clinical diagnosis and secured funding. SEM provided input on NCL disease. RGQ examined one of the affected dogs, supervised the clinical diagnosis, secured funding and drafted the manuscript. RJG conceived the mutation identification strategy, supervised PCR amplification and Sanger sequencing and drafted the manuscript. All authors read, revised critically and approved the final manuscript.

ACKNOWLEDGEMENTS

We would like to thank Ms Jennifer Barrie for her help in the preparation of the electron microscopy samples, Dr Francesco Marchesi for the histological photographies and Drs Mark McLaughlin and Intan Shafie for their help with DNA extraction. We are also grateful to the breeder and the owners of the affected dogs and of controls dogs for providing us with the samples.

373 LITTERATURE CITED

374 Abitbol M, Thibaud JL, Olby NJ, Hitte C, Puech JP, Maurer M, Pilot-Storck F, Hedan
375 B, Dreano S, Brahimi S, Delattre D, Andre C, Gray F, Delisle F, Caillaud C,
376 Bernex F, Panthier JJ, Aubin-Houzelstein G, Blot S, Tiret L. 2010. A canine
377 Arylsulfatase G (ARSG) mutation leading to a sulfatase deficiency is
378 associated with neuronal ceroid lipofuscinosis. Proceedings of the
379 National Academy of Sciences of the United States of America
380 107(33):14775-14780.
381 Aiello C, Terracciano A, Simonati A, Discepoli G, Cannelli N, Claps D, Crow YJ,
382 Bianchi M, Kitzmuller C, Longo D, Tavoni A, Franzoni E, Tessa A, Veneselli
383 E, Boldrini R, Filocamo M, Williams RE, Bertini ES, Biancheri R, Carrozzo
384 R, Mole SE, Santorelli FM. 2009. Mutations in MFSD8/CLN7 are a frequent
385 cause of variant-late infantile neuronal ceroid lipofuscinosis. Human
386 mutation 30(3):E530-540.
387 Anderson GW, Goebel HH, Simonati A. 2013. Human pathology in NCL.
388 Biochimica et biophysica acta 1832(11):1807-1826.
389 Awano T, Katz ML, O'Brien DP, Taylor JF, Evans J, Khan S, Sohar I, Lobel P,
390 Johnson GS. 2006. A mutation in the cathepsin D gene (CTSD) in American
391 Bulldogs with neuronal ceroid lipofuscinosis. Molecular genetics and
392 metabolism 87(4):341-348.
393 Cingolani P, Platts A, Wang le L, Coon M, Nguyen T, Wang L, Land SJ, Lu X, Ruden
394 DM. 2012. A program for annotating and predicting the effects of single
395 nucleotide polymorphisms, SnpEff: SNPs in the genome of Drosophila
396 melanogaster strain w1118; iso-2; iso-3. Fly 6(2):80-92.
397 Damme M, Brandenstein L, Fehr S, Jankowiak W, Bartsch U, Schweizer M,
398 Hermans-Borgmeyer I, Storch S. 2014. Gene disruption of Mfsd8 in mice
399 provides the first animal model for CLN7 disease. Neurobiology of disease
400 65:12-24.
401 DePristo MA, Banks E, Poplin R, Garimella KV, Maguire JR, Hartl C, Philippakis
402 AA, del Angel G, Rivas MA, Hanna M, McKenna A, Fennell TJ, Kernytsky
403 AM, Sivachenko AY, Cibulskis K, Gabriel SB, Altshuler D, Daly MJ. 2011. A
404 framework for variation discovery and genotyping using next-generation
405 DNA sequencing data. Nature genetics 43(5):491-498.
406 Di Fruscio G, Schulz A, De Cegli R, Savarese M, Mutarelli M, Parenti G, Banfi S,
407 Braulke T, Nigro V, Ballabio A. 2015. Lysoplex: An efficient toolkit to
408 detect DNA sequence variations in the autophagy-lysosomal pathway.
409 Autophagy 11(6):928-938.
410 Drogemuller C, Karlsson EK, Hytonen MK, Perloski M, Dolf G, Sainio K, Lohi H,
411 Lindblad-Toh K, Leeb T. 2008. A mutation in hairless dogs implicates
412 FOXI3 in ectodermal development. Science 321(5895):1462.
413 Elleder M, Kousi M, Lehesjoki AE, Mole SE, Siintola E, Topcu M. 2011. CLN7. In:
414 Mole SE, Williams RE, Goebel HH, editors. The neuronal ceroid
415 lipofuscinoses (Batten disease). 2nd ed. Oxford: Oxford University Press.
416 Faller KM, Gutierrez-Quintana R, Mohammed A, Rahim AA, Tuxworth RI, Wager
417 K, Bond M. 2015. The neuronal ceroid lipofuscinoses: Opportunities from
418 model systems. Biochimica et biophysica acta 1852(10 Pt B):2267-2278
419 Farias FH, Zeng R, Johnson GS, Wininger FA, Taylor JF, Schnabel RD, McKay SD,
420 Sanders DN, Lohi H, Seppala EH, Wade CM, Lindblad-Toh K, O'Brien DP,

421 Katz ML. 2011. A truncating mutation in ATP13A2 is responsible for
422 adult-onset neuronal ceroid lipofuscinosis in Tibetan terriers.
423 Neurobiology of disease 42(3):468-474.
424 Gilliam D, Kolicheski A, Johnson GS, Mhlanga-Mutangadura T, Taylor JF, Schnabel
425 RD, Katz ML. 2015. Golden Retriever dogs with neuronal ceroid
426 lipofuscinosis have a two-base-pair deletion and frameshift in CLN5.
427 Molecular genetics and metabolism 115(2-3):101-109.
428 Guo J, Johnson GS, Brown HA, Provencher ML, da Costa RC, Mhlanga-
429 Mutangadura T, Taylor JF, Schnabel RD, O'Brien DP, Katz ML. 2014. A
430 CLN8 nonsense mutation in the whole genome sequence of a mixed breed
431 dog with neuronal ceroid lipofuscinosis and Australian Shepherd
432 ancestry. Molecular genetics and metabolism 112(4):302-309.
433 Guo J, O'Brien DP, Mhlanga-Mutangadura T, Olby NJ, Taylor JF, Schnabel RD, Katz
434 ML, Johnson GS. 2015. A rare homozygous MFSD8 single-base-pair
435 deletion and frameshift in the whole genome sequence of a Chinese
436 Crested dog with neuronal ceroid lipofuscinosis. BMC veterinary research
437 10:960.
438 Jolly RD, Palmer DN. 1995. The neuronal ceroid-lipofuscinoses (Batten disease):
439 comparative aspects. Neuropathol Appl Neurobiol 21(1):50-60.
440 Katz ML, Farias FH, Sanders DN, Zeng R, Khan S, Johnson GS, O'Brien DP. 2011. A
441 missense mutation in canine CLN6 in an Australian shepherd with
442 neuronal ceroid lipofuscinosis. J Biomed Biotechnol 2011:198042.
443 Katz ML, Khan S, Awano T, Shahid SA, Siakotos AN, Johnson GS. 2005a. A
444 mutation in the CLN8 gene in English Setter dogs with neuronal ceroid-
445 lipofuscinosis. Biochem Biophys Res Commun 327(2):541-547.
446 Katz ML, Narfstrom K, Johnson GS, O'Brien DP. 2005b. Assessment of retinal
447 function and characterization of lysosomal storage body accumulation in
448 the retinas and brains of Tibetan Terriers with ceroid-lipofuscinosis. Am J
449 Vet Res 66(1):67-76.
450 Kousi M, Lehesjoki AE, Mole SE. 2012. Update of the mutation spectrum and
451 clinical correlations of over 360 mutations in eight genes that underlie the
452 neuronal ceroid lipofuscinoses. Human mutation 33(1):42-63.
453 Kowalewski B, Heimann P, Ortkras T, Lullmann-Rauch R, Sawada T, Walkley SU,
454 Dierks T, Damme M. 2015. Ataxia is the major neuropathological finding
455 in arylsulfatase G-deficient mice: similarities and dissimilarities to
456 Sanfilippo disease (mucopolysaccharidosis type III). Human molecular
457 genetics 24(7):1856-1868.
458 Kowalewski B, Lamanna WC, Lawrence R, Damme M, Stroobants S, Padva M,
459 Kalus I, Frese MA, Lubke T, Lullmann-Rauch R, D'Hooge R, Esko JD, Dierks
460 T. 2012. Arylsulfatase G inactivation causes loss of heparan sulfate 3-O-
461 sulfatase activity and mucopolysaccharidosis in mice. Proceedings of the
462 National Academy of Sciences of the United States of America
463 109(26):10310-10315.
464 Kuwamura M, Hattori R, Yamate J, Kotani T, Sasai K. 2003. Neuronal ceroid-
465 lipofuscinosis and hydrocephalus in a chihuahua. J Small Anim Pract
466 44(5):227-230.
467 Li H, Durbin R. 2009. Fast and accurate short read alignment with Burrows-
468 Wheeler transform. Bioinformatics 25(14):1754-1760.

McKenna A, Hanna M, Banks E, Sivachenko A, Cibulskis K, Kernytsky A, Garimella K, Altshuler D, Gabriel S, Daly M, DePristo MA. 2010. The Genome Analysis Toolkit: a MapReduce framework for analyzing next-generation DNA sequencing data. Genome research 20(9):1297-1303.

Melville SA, Wilson CL, Chiang CS, Studdert VP, Lingaas F, Wilton AN. 2005. A mutation in canine CLN5 causes neuronal ceroid lipofuscinosis in Border collie dogs. Genomics 86(3):287-294.

Mole SE, Williams RE. 2001 [Updated 2013]. Neuronal Ceroid-Lipofuscinoses. In: Pagon RA, Adam MP, Ardinger HH, Wallace SE, Amemiya A, Bean LJH, Bird TD, Dolan CR, Fong CT, Smith RJH, Stephens K, editors. GeneReviews(R) [Internet]. Seattle (WA): University of Washington, Seattle. Available from: http://www.ncbi.nlm.nih.gov/books/NBK1428/.

Nakamoto Y, Yamato O, Uchida K, Nibe K, Tamura S, Ozawa T, Ueoka N, Nukaya A, Yabuki A, Nakaichi M. 2011. Neuronal ceroid-lipofuscinosis in longhaired Chihuahuas: clinical, pathologic, and MRI findings. J Am Anim Hosp Assoc 47(4):e64-70.

Rac R, Giesecke PR. 1975. Letter: Lysosomal storage disease in chihuahuas. Australian veterinary journal 51(8):403-404.

Sanders DN, Farias FH, Johnson GS, Chiang V, Cook JR, O'Brien DP, Hofmann SL, Lu JY, Katz ML. 2010. A mutation in canine PPT1 causes early onset neuronal ceroid lipofuscinosis in a Dachshund. Molecular genetics and metabolism 100(4):349-356.

Shacka JJ. 2012. Mouse models of neuronal ceroid lipofuscinoses: useful pre-clinical tools to delineate disease pathophysiology and validate therapeutics. Brain Res Bull 88(1):43-57.

Wohlke A, Philipp U, Bock P, Beineke A, Lichtner P, Meitinger T, Distl O. 2011. A one base pair deletion in the canine ATP13A2 gene causes exon skipping and late-onset neuronal ceroid lipofuscinosis in the Tibetan terrier. PLoS Genet 7(10):e1002304.

500 FIGURE LEGENDS

501

502 Figure 1: Pedigree of the family of Chihuahua dogs. Solid figures represent affected
503 dogs, whereas plain figures are clinically unaffected dogs. Squares represent males
504 and circles females. Genotypes of the tested dogs are mentioned under each figure
505 with WT = wild-type allele and Del = *MFSD8*:c.843delT:p.Phe282Leufs13* allele.

506

507 Figure 2: Magnetic resonance imaging and histological findings of the male dog. A:
508 Sagittal T2-weighted image of the brain. Note the marked generalised cerebral
509 atrophy. B: H&E staining of the cerebellum at high magnification showing inclusions
510 within the Purkinje cells (arrows). C & D: Periodic acid-Schiff (C) and Luxol Fast
511 Blue (D) staining of brainstem neurons at high magnification. E:Fluorescence cryostat
512 section of the cerebral cortex showing abundant autofluorescent inclusions. F & G:
513 Lysosomal staining by use of anti-LAMP-1 antibody of the cerebellum of the affected
514 dog (F) and of a control dog (G). H: Immunostaining against GFAP (brainstem). I:
515 Electron microscopy of the storage bodies from the cerebral cortex. Note the mixed
516 nature of the inclusions with curvilinear (*) and rectilinear (arrow) profiles. J. H&E
517 staining of a retinal section. Note the marked depletion of the ganglion cells.
518 NFL: nerve fiber layer. GCL: ganglion cell layer. IPL: inner plexiform layer. INL:
519 inner nuclear layer. OPL: outer plexiform layer. ONL: outer nuclear layer. RL:
520 receptor layer.

521

522 Figure 3: H&E sections of the vermis of the cerebellum of the affected dog (A1 and
523 A2) and of a control dog (B1 and B2) at low and high magnification. Note the marked
524 depletion in granule cells in the affected dog (the blue line in each panel spans the

granular layer). This results in an overall marked atrophy of the cerebellar cortex. In the affected dog, there is a moderate decrease in number of Purkinje cells (*), which show signs of degeneration. NB: in the control dog, at high magnification (B2), the white lamina is not seen due to the normal thickness of the granule cell layer, preventing visualisation of the white lamina in the same image as the three layers of cerebellar grey matter.

Figure 4: Sequence traces showing a small portion of the genomic DNA of the Chihuahua dogs shown in the pedigree (Fig. 2), and centered around the mutation of interest (*MFSD8*:c.843delT:p.Phe282Leufs13*). All sequences are aligned against the canine reference genome (CanFam3.1).

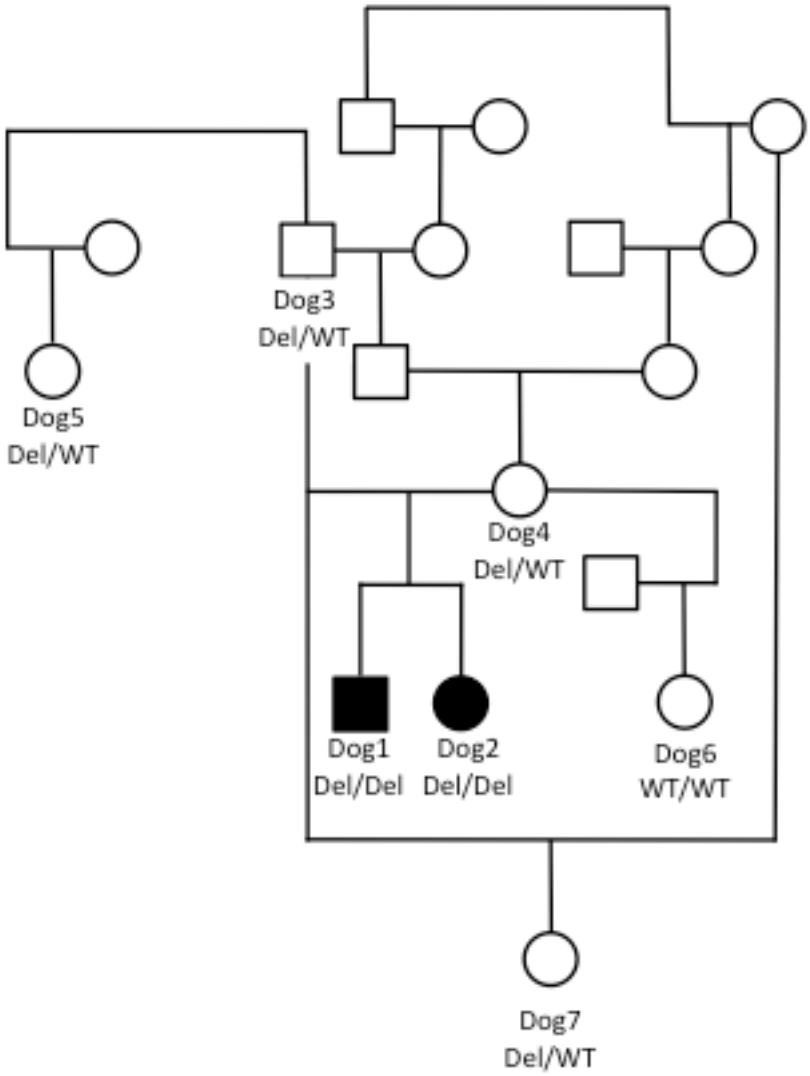

536
537 **Figure 1**
538

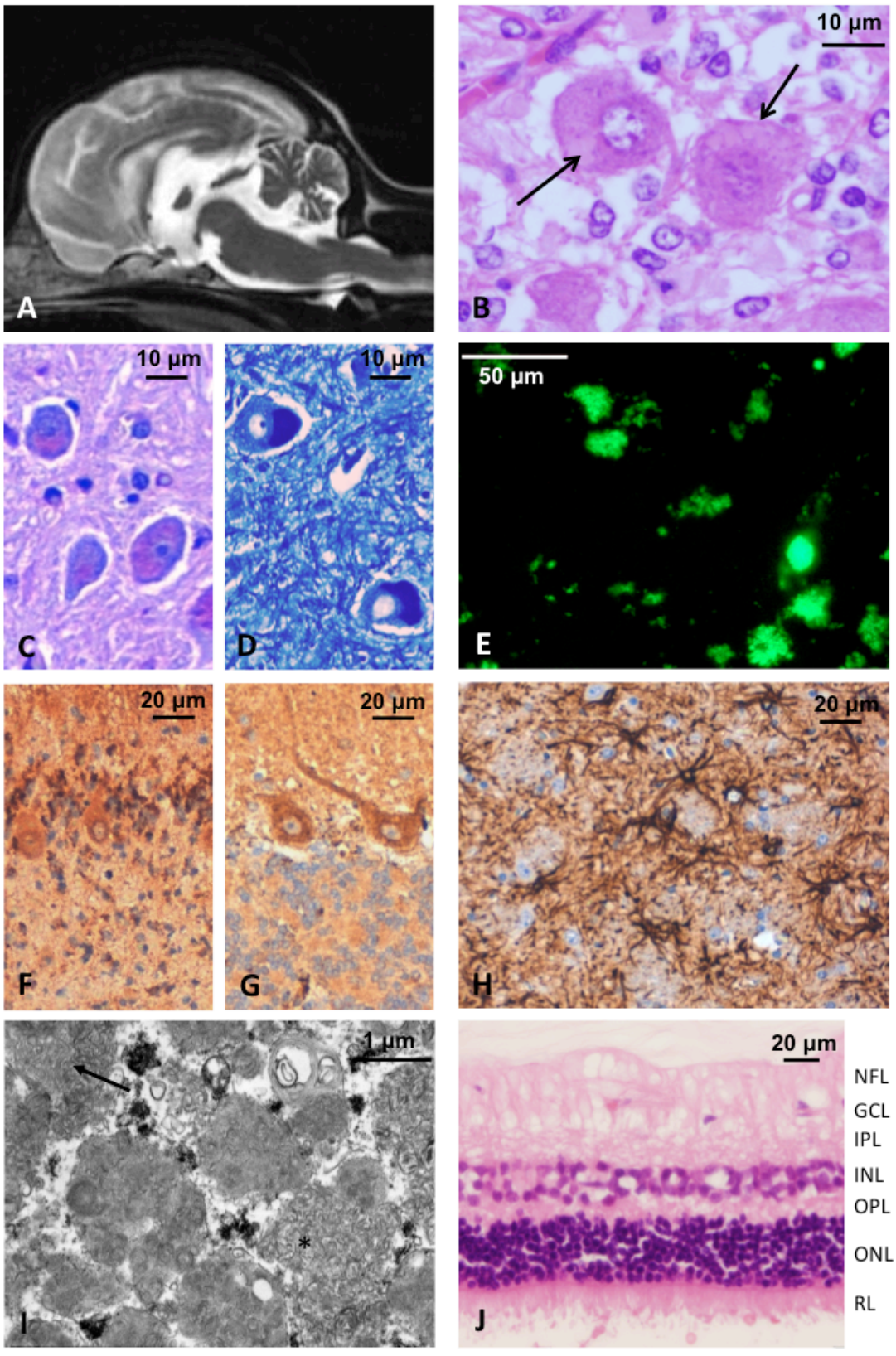
A
B
10 µm
C
10 µm
D
10 µm
E
50 µm
F
20 µm
G
20 µm
H
20 µm
I
1 µm
J
20 µm
NFL
GCL
IPL
INL
OPL
ONL
RL

Figure 2

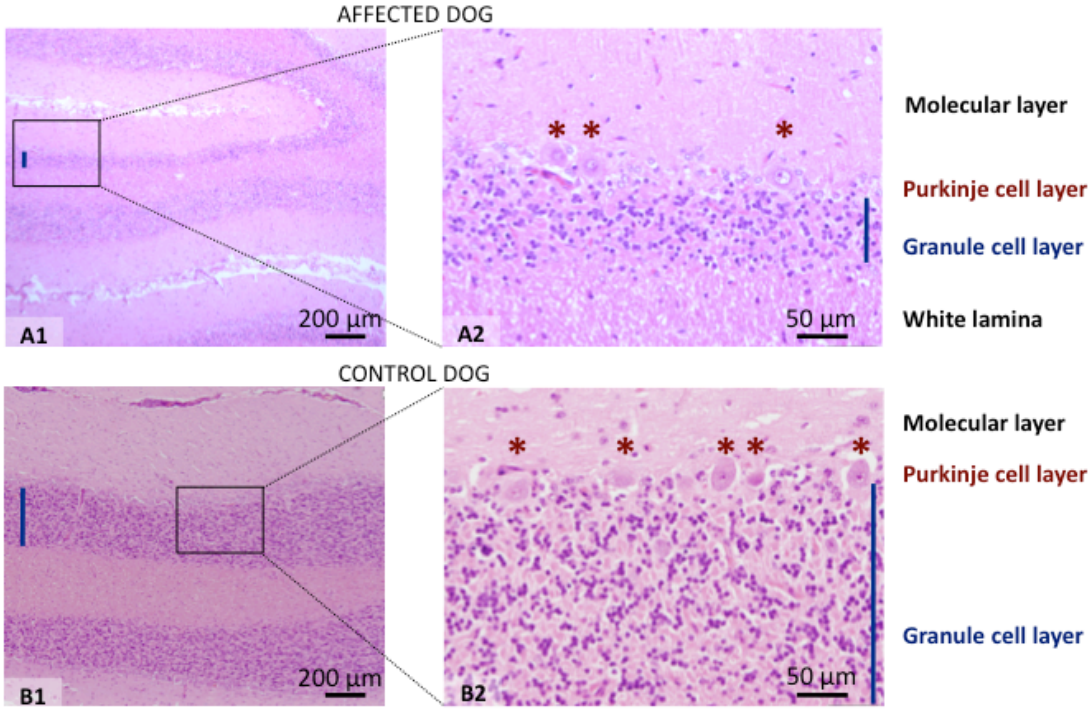
AFFECTED DOG
A1
200 µm
A2
50 µm
Molecular layer
Purkinje cell layer
Granule cell layer
White lamina
CONTROL DOG
B1
200 µm
B2
50 µm
Molecular layer
Purkinje cell layer
Granule cell layer

Figure 3

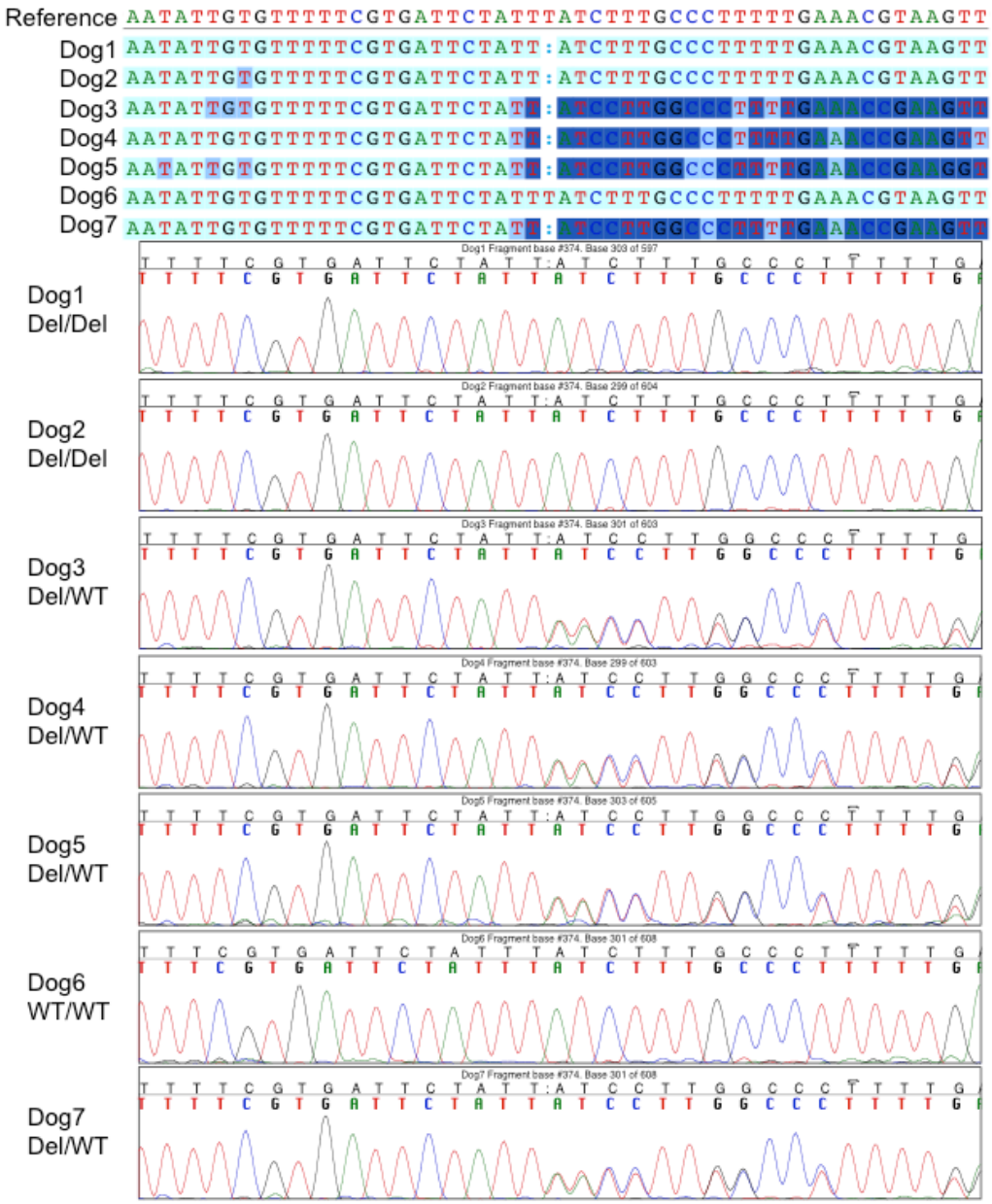
Reference AATATTGTGTTTTTCGTGATTCTATTTATCTTTGCCCTTTTTGAAACGTAAGTT
Dog1 AATATTGTGTTTTTCGTGATTCTATT:ATCTTTGCCCTTTTTGAAACGTAAGTT
Dog2 AATATTGTGTTTTTCGTGATTCTATT:ATCTTTGCCCTTTTTGAAACGTAAGTT
Dog3 AATATTGTGTTTTTCGTGATTCTATT:ATCCTTGGCCCTTTTGAAACCGAAGTT
Dog4 AATATTGTGTTTTTCGTGATTCTATT:ATCCTTGGCCCTTTTGAAACCGAAGTT
Dog5 AATATTGTGTTTTTCGTGATTCTATT:ATCCTTGGCCCTTTTGAAACCGAAGGT
Dog6 AATATTGTGTTTTTCGTGATTCTATTTATCTTTGCCCTTTTTGAAACGTAAGTT
Dog7 AATATTGTGTTTTTCGTGATTCTATT:ATCCTTGGCCCTTTTGAAACCGAAGTT
Dog1 Del/Del
Dog2 Del/Del
Dog3 Del/WT
Dog4 Del/WT
Dog5 Del/WT
Dog6 WT/WT
Dog7 Del/WT

Figure 4

547 *Table I. Table of Primary Antibodies Used.*

548

Antigen	**Description of Immunogen**	**Source, Host Species, Cat. #, Clone or Lot#, RRID**	**Concentration Used**
LAMP-1	Lysosomal associated membrane protein 1	Abcam, mouse monoclonal, Cat# ab25630 RRID : AB_470708	1:200
Glial fibrillary acidic protein (GFAP)	GFAP isolated from bovine spinal cord	Dako, Rabbit monoclonal, Cat# Z0334, RRID:AB_2314535	1:1000

549

550

Table II: Homozygous variants in the coding region or splicing areas of previously known NCL genes used for Sanger sequencing confirmation and segregation analyses.

Gene (transcript)	Variant location	Primers
ARSG *(XM_005624176.1)*	p.Val262Asp	F: 5'-ACCTCTTGGCTTTCCCATTG-3' R: 5'-CAGGGAGCTAGCTGGGTTTT-3'
CLN6 *(NM_001011888.1)*	p.Lys29Arg	F: 5'-CACAGTGCTTCCCGCAAC-3' R: 5'-CACCAAAACCGCATCCTACT-3'
TPP1 *(NM_001013847.1)*	Splice site (rs22973585)	F: 5'-GCTCACAGTGTGCACATGTG-3' R: 5'-GAGTACCTGATGAGTGCCGG-3'
CLN7/ MFSD8 *(XM_533294.4)*	c.843delT; p.F282Lfs13*	F: 5'-ATCTCCTGGGAAGAAAATTCAC-3' R: 5'-TTAAATCATGGCACTGAAGTTTT-3'

Only the mutation identified in MFSD8:c.843delT:p.Phe282Leufs13 segregated with the disease in the studied family*.

560 *Table III: Comparison of the phenotypes of human CLN7 disease, the Mfsd8*$^{(tm1a/tm1a)}$

561 *mouse model (Damme et al., 2014) and the canine model described here and in the*

562 *literature.*

Neuropathological features	**CLN7 disease (humans)**	***Mfsd8*$^{(tm1a/tm1a)}$ (mice) (Damme et al 2014)**	**CLN7 disease (canine)**
Retinal degeneration	Yes	Yes	Yes (this report, Kuwamura *et al.*, 2003)
Accumulation of SCMAS (Sub-unit C of mitochondrial ATP synthase)	Yes	Yes	Not performed
Accumulation of autofluorescent ceroid lipopigments	Yes	Yes	Yes (this report; Kuwamura *et al.*, 2003; Guo *et al.*, 2015)
Astrogliosis	Yes	Only mildly	Yes (this report, Guo *et al.*, 2015; Kuwamura *et al.*, 2003; Nakamoto *et al.*, 2011)
Generalised seizures	Yes	No	No (this report; Guo *et al.*, 2015; Kuwamura *et al.*, 2003) Suspected partial seizure (jaw chomping) (Rac *et al.*, 1975) Terminal stage (Nakamoto *et al.*, 2011)
Myoclonus/ataxia	Yes	Yes	Yes (ataxia) (this report; Guo *et al.*, 2015; Rac *et al.*, 1975; Nakamoto *et al.*, 2011)
Neuronal loss / brain atrophy	Yes	No	Yes (this report, Guo *et al.*, 2015; Rac *et al.*, 1975; Nakamoto *et al.*, 2011; Kuwamura *et al.*, 2003)
Premature death	Yes (mean age 11.5 years) (Kousi et al	No	Yes (euthanasia as not compatible with life) –

	2009)	~ 1.5 - 2 years (lifespan of a Chihuahua or a Chinese Crested dog > 12 years) (this report; Kuwamura *et al*., 2003; Rac *et al*., 1975; Nakamoto *et al*., 2011; Guo *et al*., 2015).

563 *Table adapted from Damme et al. (2014)*